



An assessment of landslide susceptibility in the Faifa area, Saudi Arabia, using remote sensing and GIS techniques

T. Alharbi^{1,2}, M. Sultan¹, S. Sefry³, R. ElKadiri¹, M. Ahmed^{1,4}, R. Chase¹, A. Milewski⁵, M. Abu Abdullah³, M. Emil¹, and K. Chounaird¹

¹Geosciences, Western Michigan University, 1903 W. Michigan Avenue, Kalamazoo, MI 49008, USA

²Geology and Geophysics, King Saud University, 2455, 11451 Riyadh, Saudi Arabia

³Saudi Geological Survey, 21514 Jeddah, Saudi Arabia

⁴Geology, Faculty of Science, Suez Canal University, 41522 Ismailia, Egypt

⁵Geology, University of Georgia, Geography-Geology Building, 210 Field Street, Athens, GA 30602, USA

Correspondence to: M. Sultan (mohamed.sultan@wmich.edu)

Received: 18 July 2013 – Published in Nat. Hazards Earth Syst. Sci. Discuss.: 25 November 2013

Revised: – Accepted: 30 April 2014 – Published: 23 June 2014

Abstract. An integrated approach was adopted over Faifa Mountain and its surroundings, in Saudi Arabia, to identify landslide types, distribution, and controlling factors, and to generate landslide susceptibility maps. Given the inaccessibility of the area, we relied on remote sensing observations and GIS-based applications to enable spatial analysis of data and extrapolation of limited field observations. Susceptibility maps depicting debris flows within ephemeral valleys (Type I) and landslides caused by failure along fracture planes (Type II) were generated. Type I susceptibility maps were generated applying linear relationships between normalized difference vegetation index (NDVI) and threshold slope values (30°), both of which were extracted over known debris flow locations. For Type II susceptibility maps, landslides were predicted if fracture planes had strike values similar to (within 20°) those of the slope face strike and dip angles exceeding the friction, but not the slope angles. Comparisons between predicted and observed debris flows yielded success rates of 82 % (ephemeral valleys); unverified predictions are interpreted as future locations of debris flows. Our approach could serve as a replicable model for many areas worldwide, in areas where field measurements are difficult to obtain and/or are cost prohibitive.

1 Introduction

The Red Sea hills of the Arabian Peninsula consist of a complex of volcano-sedimentary igneous and metamorphic rocks that were formed by the accretion of island arcs and closure of interleaving oceanic arcs 550–950 Ma (Stoeser and Camp, 1985). The uplift associated with the opening of the Red Sea some 30 million years ago exposed this complex along the length of the Red Sea on its African and Arabian sides (Wolfenden et al., 2004). The basement complex is unconformably overlain by Paleozoic, Mesozoic, and lower Tertiary sedimentary successions (Fig. 1a) (Agar, 1987). The study area, Faifa Mountain and its surroundings in the Jazan region (latitude: $16.5\text{--}17.7^\circ$ N; longitude: $42.0\text{--}43.8^\circ$ E), is located within the basement complex of the Red Sea hills to the north of the Saudi–Yemen border (Alehaideb, 1985; Abou Ouf and El Shater, 1992). In the study area, highly deformed rocks of variable compositions (granite gneiss, amphibolite, phyllite, quartzite, schist) are intruded by a massive syenite intrusion, and the area is dissected by fault systems that run in various directions. Elevations are high, reaching up to 1800 m a.m.s.l. (above mean sea level) at the top of the mountains, and as low as 230 m a.m.s.l. at the foot of the mountains (Fig. 2a). Precipitation is high (up to 800 mm year^{-1} ; Fig. 1b) and slopes are steep (up to 71° ; Fig. 2b).

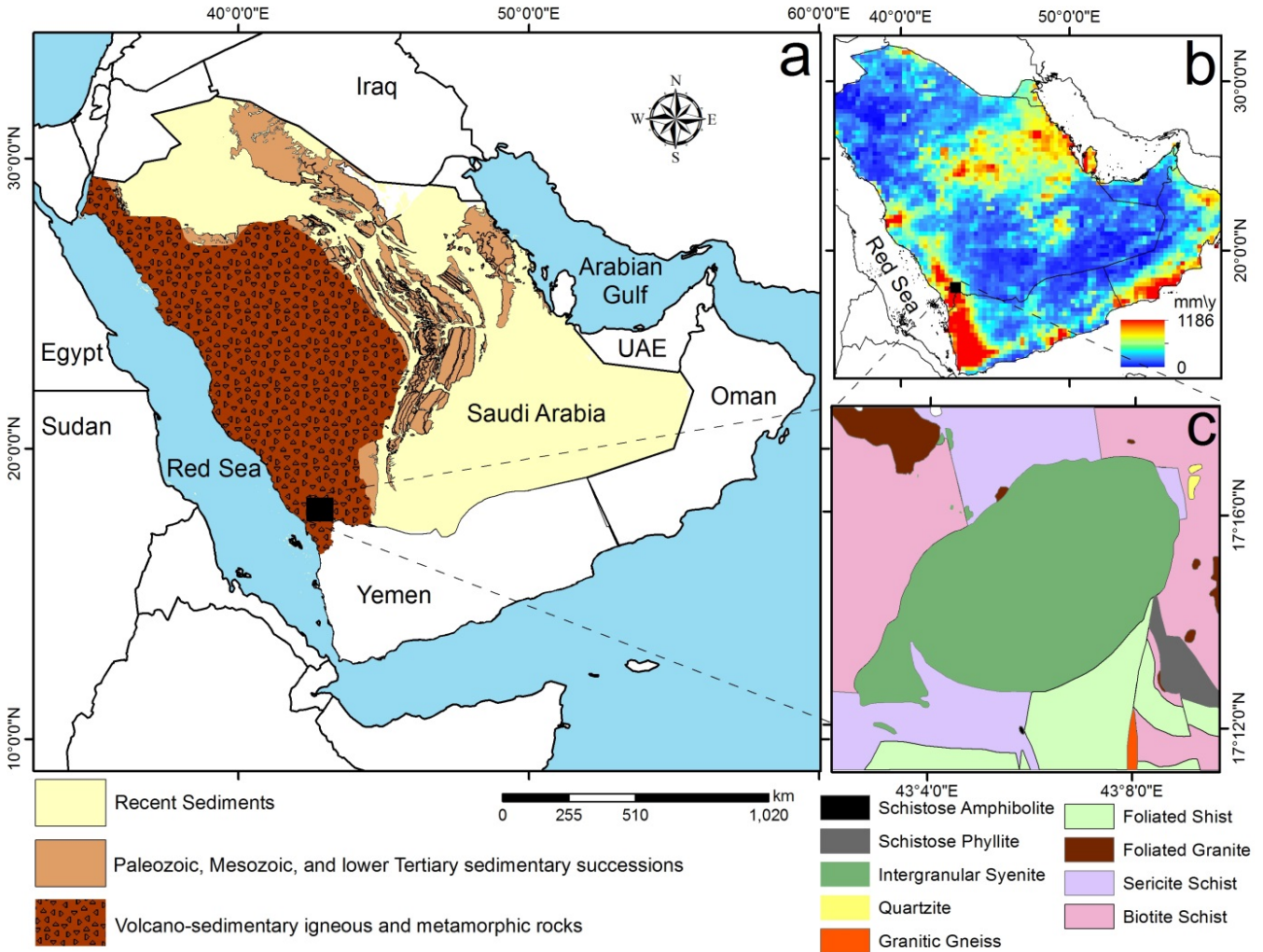


Figure 1. (a) Location map showing the Faifa area in the Arabian Peninsula, the distribution of volcano-sedimentary igneous and metamorphic rocks, and overlying Paleozoic, Mesozoic, and lower Tertiary sedimentary successions in the Kingdom of Saudi Arabia. (b) Total annual precipitation (January 2011 to December 2011) extracted from TRMM 3-hourly data for the Arabian Peninsula. (c) Main geologic map showing the rock units in the Faifa area (modified after Fairer, 1985).

The discovery of oil in the Kingdom of Saudi Arabia signaled the beginning of an important era, in which new urban centers and networks of highways were constructed. Faifa Mountain and its surroundings were no exception. These areas witnessed the construction of highways, roadcuts, and bridges to connect the remote mountainous terrain to the coastal plain. Given the high levels of precipitation over the Faifa area, the steep gradient, and the intensified construction phase, landslides are becoming problematic. In this paper, we examine the distribution and nature of landslides, investigate the factors controlling their development, and use this information to construct landslide susceptibility maps for the Faifa area. Our approach is largely based on observations extracted from remotely acquired data sets and field data.

2 Methodology

Our approach involves the following steps: (1) examination of known landslide locations in the field and/or from high-resolution remote sensing data sets, and characterization of their type; (2) extraction of criteria to enable identification of known landslide locations using remote sensing data sets; (3) use of the selected criteria to identify areas where similar landslide types could occur elsewhere in the study area; and (4) refinement and validation of predictions. Step 3 entails the generation of susceptibility maps that show the relative likelihood for the occurrence of each of the identified landslide types across the investigated area. On these maps, the likelihood for the occurrence of a landslide is dictated by the intensity of one or more of the factors controlling landslide occurrence. Examples of these factors include slope

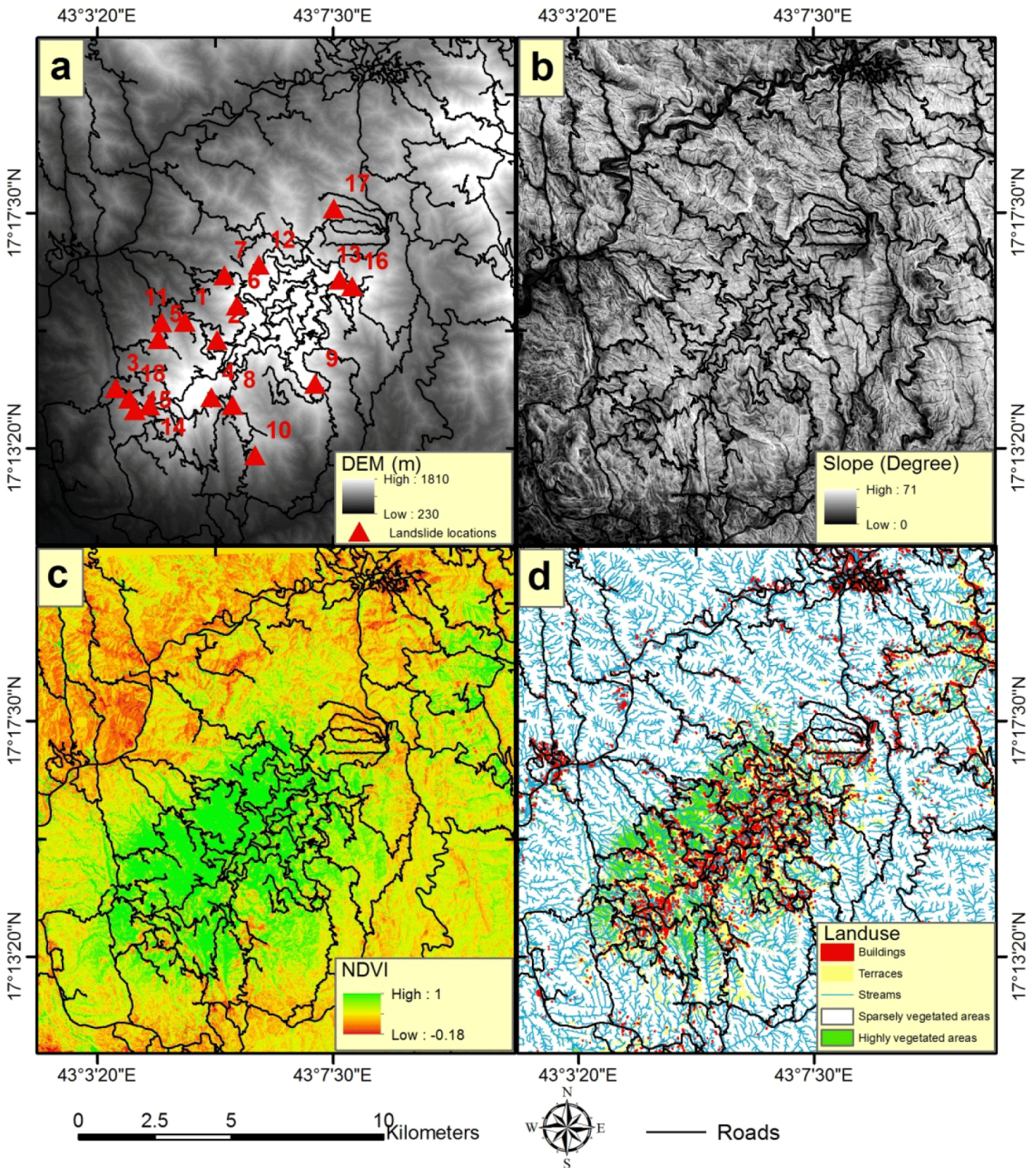


Figure 2. (a) Location map showing the distribution of landslides that were visited in the field (1–3, 6, 8, 10, 13–18) and a selected suite of similar landslides that were extracted from remotely acquired data (4, 5, 7, 9, 11, 12); background DEM image. (b) Map showing the distribution of slopes in the study area. (c) Color-coded NDVI image generated from SPOT image. (d) Land use map for the study area showing the distribution of roads, buildings, and terraces extracted manually from Google Earth images; stream networks extracted from 10 m DEM; and highly vegetated areas (NDVI: 0.09 to 1) and sparsely vegetated areas (NDVI: –0.18 to 0.09) generated from SPOT imagery. Also shown are the distributions of road networks.

angle and direction, fracture plane dip angle and dip direction, vegetation intensity, and man-made structures (Cruden and Varnes, 1996).

To conduct steps 1 through 4, we had to produce many derived image products that display important topographic and spectral characteristics of interest that could be used to identify existing landslide locations and areas prone to landslide development. Examples of these characteristics include disruption of contoured elevations, decrease in vegetation, and high spectral reflectance within areas affected by landslides. Investigating the intensity of vegetation in an area was possible as a result of examining normalized difference vegetation index (NDVI) images; these were extracted from spectral reflectance images, which were in turn derived from raw DN (digital number images) of SPOT (Système Pour l'Observation de la Terre) multispectral images. Additional products were generated to evaluate the potential losses in human life and property that are associated with the identified landslide types. Examples of these additional products include maps showing the intersections of debris flows with houses and roads. These and many other products were generated and hosted in a web-based geographic information system (GIS) (<http://www.esrs.wmich.edu/webmap>). Constructing the web-based GIS made it possible to correlate spatial and temporal coregistered data sets and the development of conceptual models to identify the conditions for landslide development, predict the areas in which landslides could occur, and identify locations for fieldwork to examine predictions and refine the adopted methodologies.

2.1 Generation of a web-based GIS

The adopted approach entails (1) compilation of relevant data sets, and (2) development of a web-based GIS to organize and manage the data sets and provide a platform for users to access, visualize, and analyze the accumulated data types for the study area. The adopted system is a hybrid system that takes advantage of the existing tools and data sets in Google Maps, applies Python scripts to generate custom tools, and uses the ArcGIS server to host the services.

Three types of data sets collected for the study were also included in the web-based GIS (folder name: Faifa): (1) published data sets (geologic maps, remote sensing data); (2) derived products (e.g., false color images, contour maps); and (3) field data (e.g., dip direction and dip amount of fracture planes). Susceptibility maps were extracted from the analysis of the above-mentioned data sets and were also incorporated in the web-based GIS. All of the data sets described above are included in seven subfolders. (1) The “Topography” subfolder includes (a) a 10 m digital elevation model (DEM) (Fig. 2a) that was extracted from digital topographic contour maps provided by the Saudi Geological Survey (SGS); (b) a hillshade map; and (c) a slope map (Fig. 2b). (2) The “Remote Sensing” subfolder includes (a) a visible Google Earth image acquired in April 2010 (spatial resolution: 0.56 m);

(b) a false-color composite image from GeoEye images (blue: band 1; green: band 2; red: band 3) (spatial resolution: 0.5 m); (c) Shuttle Imaging Radar band C (SIR-C) (spatial resolution: 50 m) data; (d) NDVI extracted from SPOT multispectral images (spatial resolution: 2.5 m), which provides a measure for the intensity of vegetation (Fig. 2c) (the higher the NDVI values for a picture element, the more extensive the vegetation, and vice versa; Rouse, 1973); (e) an Advanced Spaceborne Thermal Emission and Reflection Radiometer (ASTER) false-color composite (blue: band 1; green: band 2; red: band 3) (spatial resolution: 15 m); (f) a Landsat Thematic Mapper (TM) false-color composite ratio image (blue: 5/4; green: 5/1, red: 5/7) (spatial resolution: 30 m). (3) The “Geology” subfolder includes (a) a scanned and digitized geologic map (Fairer, 1985) (scale 1 : 250 000); (b) the distribution of faults/fractures extracted from geologic maps (Fairer, 1985), ASTER, Landsat TM, SIR-C, and DEM; and (c) fracture dip aspect (direction) and amount, measured along the major roads by SGS geologists. (4) The “Land Use” subfolder contains digitized buildings, roads, naturally vegetated areas, bare soils, and terraces extracted from Google Earth and GeoEye images (Fig. 2d). (5) The “Hydrology” subfolder includes products that were extracted from digital 10 m DEM: (a) stream distribution (Fig. 2d) generated using standard techniques for stream delineation, such as the TOPAZ technique (Garbrecht and Martz, 1997); and (b) flow accumulation that provides a count for the number of pixels that drain toward a certain pixel (Chang, 2006). (6) The “Field Data” subfolder is comprised of the types and locations of the landslide sites (Fig. 2a) that were visited in the field (January 2010 and January 2012). (7) The “Hazard” subfolder includes various susceptibility maps generated for each of the two main types of landslides identified in the study area: those related to debris flows and those related to failure on fracture planes.

2.2 Landslide types in the study area

Our observations from field trips 1 and 2 (Fig. 3) and examination of remotely acquired data sets led us to identify two major types of landslides: those related to debris flows (Fig. 4a) and those related to failure along fracture planes (Fig. 4b). In the following sections, we discuss the criteria by which we identify each of these landslide types from field and remotely acquired data and the methodology used to generate susceptibility maps for each of the identified landslide types.

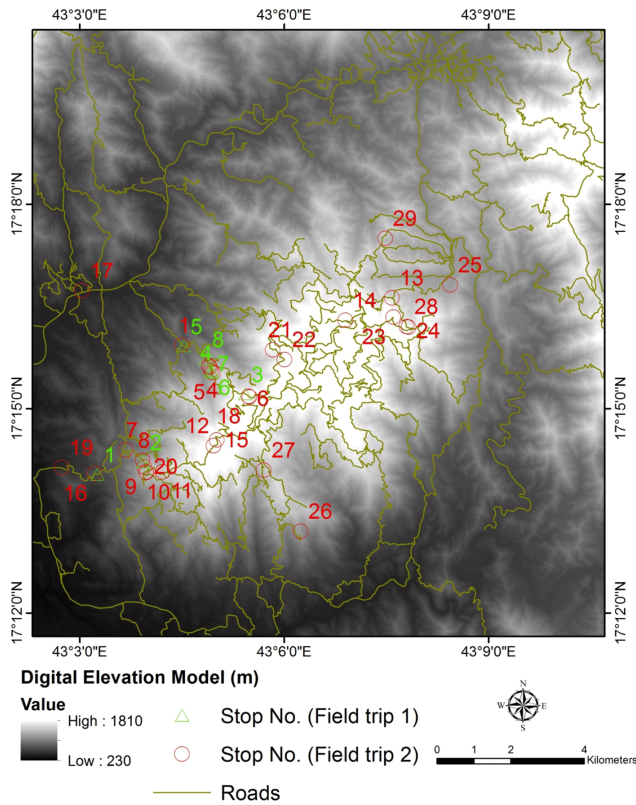


Figure 3. Location map showing the stops visited throughout field trips 1 and 2.

2.2.1 Debris flows within ephemeral valleys

Debris flows often have high densities, consisting of over 80 % solids by weight, and may exceed the density of wet concrete (Hutchinson, 1988). Debris flow occurs during torrential runoff following exceptional rainfalls. Soils on steep slopes that are not protected by vegetation are prone to debris flows (Cruden and Varnes, 1996).

Our observations from field trip 1 and examination of remotely acquired data sets led us to believe that a number of the visited landslides were caused by debris flows that originated with abrupt floods of water that undermined and incorporated sediments. This conclusion is supported by (1) the localization of debris along discrete channels; (2) the fact that the landslides are all at high elevations (> 800 m a.m.s.l.), where the slopes are quite steep (35 to 38°); and (3) the fact that precipitation over these steep mountains is high (up to 850 mm yr⁻¹) (Fig. 1b) and will be channeled toward the lowlands by the ephemeral valleys (Cruden and Varnes, 1996). Given the steep surface gradient in the study area and the high precipitation over the mountainous area, one would expect a heavy sediment load to be carried to the lowlands by the ephemeral streams crosscutting these mountains.

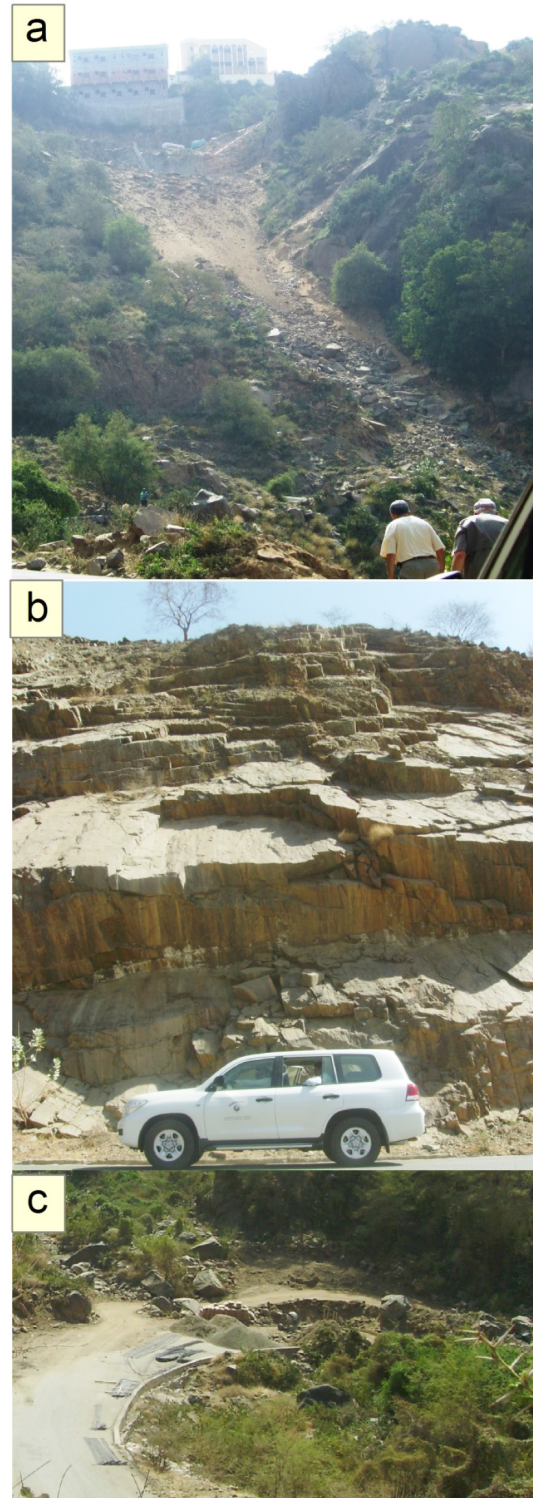


Figure 4. Field photographs taken throughout field trips 1 and 2: (a) landslide caused by debris flows within an ephemeral valley; (b) area prone to landslide development by failure along fracture planes that dip towards the road; and (c) intersection of debris flow with road.

One would expect that, in general, the steeper the slope is along the identified streams, the more likely it is for a debris flow to occur. The mean slope in the area is 23° and the standard deviation is 13° . The steepest slopes are found on the mountainsides surrounding the valleys. Areas over these steep-sloped mountainsides are prone to mass movement (i.e., landslides) initiated by debris flow.

The less the vegetation there is, the more likely it is that the stream will be effective in transporting debris downslope (Horton, 1933; Scott, 1971; Wells et al., 1987; Weirich, 1989; Florsheim et al., 1991). Only barren or nearly barren slopes along the identified stream were considered to be subject to debris flows. The NDVI values (Fig. 2c) for the study area range from -0.18 to $+1.0$. Areas with NDVI values of -0.1 to 0.09 are usually assumed to be barren rocks or dry soils (Jackson and Huete, 1991). Areas of high NDVI (shades of green) are less prone to debris flows, whereas areas of low NDVI values (shades of brown) are more prone to debris flows. During field trip 2, we visited areas with NDVI values of 0.09 or less and found that all of these areas were barren or had very sparse vegetation.

The third condition has to do with the presence or absence of terraces. In some of the steeply-sloped areas, the locals modify the slopes by building more stable structures called terraces. These terraces are concentrated at higher elevations in the Faifa area. They enhance infiltration and reduce runoff (Naderman et al., 1990). Debris flows are less likely to occur in areas where terraces are established. Based on our field observations and analysis of Google Earth images, we reached the conclusion that areas covered by terraces are stable areas that are not prone to debris flows. Figure 2d shows the distribution of terraces in the study area.

We extracted a relationship for the study area that adequately describes the interplay between the intensity of vegetation and the steepness of the slope. Using known locations of debris flows (from field and satellite observations), we extracted the slopes and NDVI values for picture elements (pixels) that we identified as representing the onset points for each of these debris flows. Areas susceptible to the development of debris flow had to meet a number of conditions: low NDVI, high slope angle, and presence along mapped stream lines and away from areas mapped as terraces. In defining the stream lines, a threshold-contributing area of 25 pixels (area: 2500 m^2) was required. The extracted slopes ranged from 30 to 42° and averaged 35° , whereas the NDVI values ranged from -0.04 to 0.24 and averaged 0.07 . A linear regression was then used to identify the equation of a straight line that best fit the points with the steepest slope and the smallest NDVI values (Fig. 5). Knowing the equation of the straight line, we then substituted NDVI and slope values for all pixels of all streams in the equation to test whether the examined stream pixel is on the line (value = 0), above the line (value: negative), or below the line (value: positive). A susceptibility map was then constructed from pixels that were found on or below the line; the selected points had slope values that

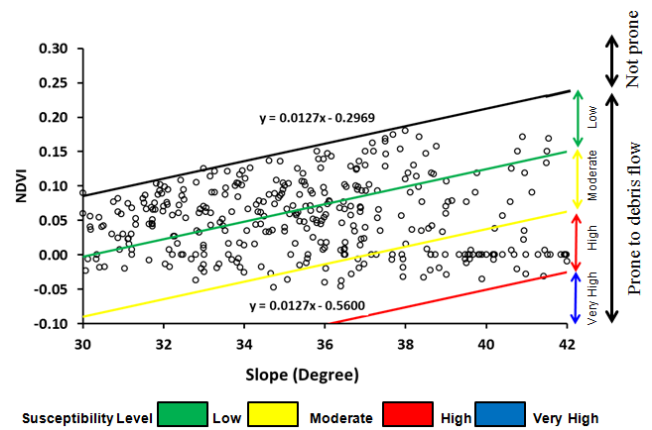


Figure 5. NDVI versus slope values for the debris flows that were verified in the field and/or by examination of Google Earth images. Also shown is a regression line that separates points prone to landslide (below line) from others that are not prone to debris flows (above line) and susceptibility levels expressed as a function of distance from the regression line.

exceeded a threshold value of 30° , the minimum observed slope angle for debris flows visited in the field (Fig. 6). Figures 5 and 6 reflect differences in susceptibility levels as a function of the distance from the regression line within areas identified on Fig. 5 as being prone to debris flow. Inspection of Fig. 5 shows that as slope values increase and/or NDVI values decrease, points become progressively separated from the regression line and more susceptible to debris flow. The constructed susceptibility map represents the locations along mapped stream lines that are susceptible to the development of debris flow. Points that fell above the line were considered to be unsusceptible to debris flow. An additional condition was enforced: the points that were found to be susceptible to debris flow had to be outside the areas mapped as terraces.

Using the criteria listed above, a susceptibility map was constructed showing the distribution of areas (1405 locations) that are prone to debris flows (hereafter referred to as predicted debris flows) (Fig. 6a). Examination of Fig. 6b and c demonstrates the correspondence between the observed and predicted debris flows. Comparisons between the distribution of a subset of the predicted flows (500 debris flows extracted using a random number generator) and the debris flows observed in the field and from Google Earth images shows a success rate of 82 %, where the predicted flows exceeded the observed flows. These additional locations probably mark potential areas where debris flows could be triggered in the future. Similar comparisons between the distributions of a subset of random areas identified as being non-prone to debris flow and the observed debris flows in the field and from Google Earth images yielded a success rate of 99.2 %.

Debris flows could pose a risk to human life and property if these flows intersect roads and houses, and if there were no or inadequate retaining walls in place. In both cases,

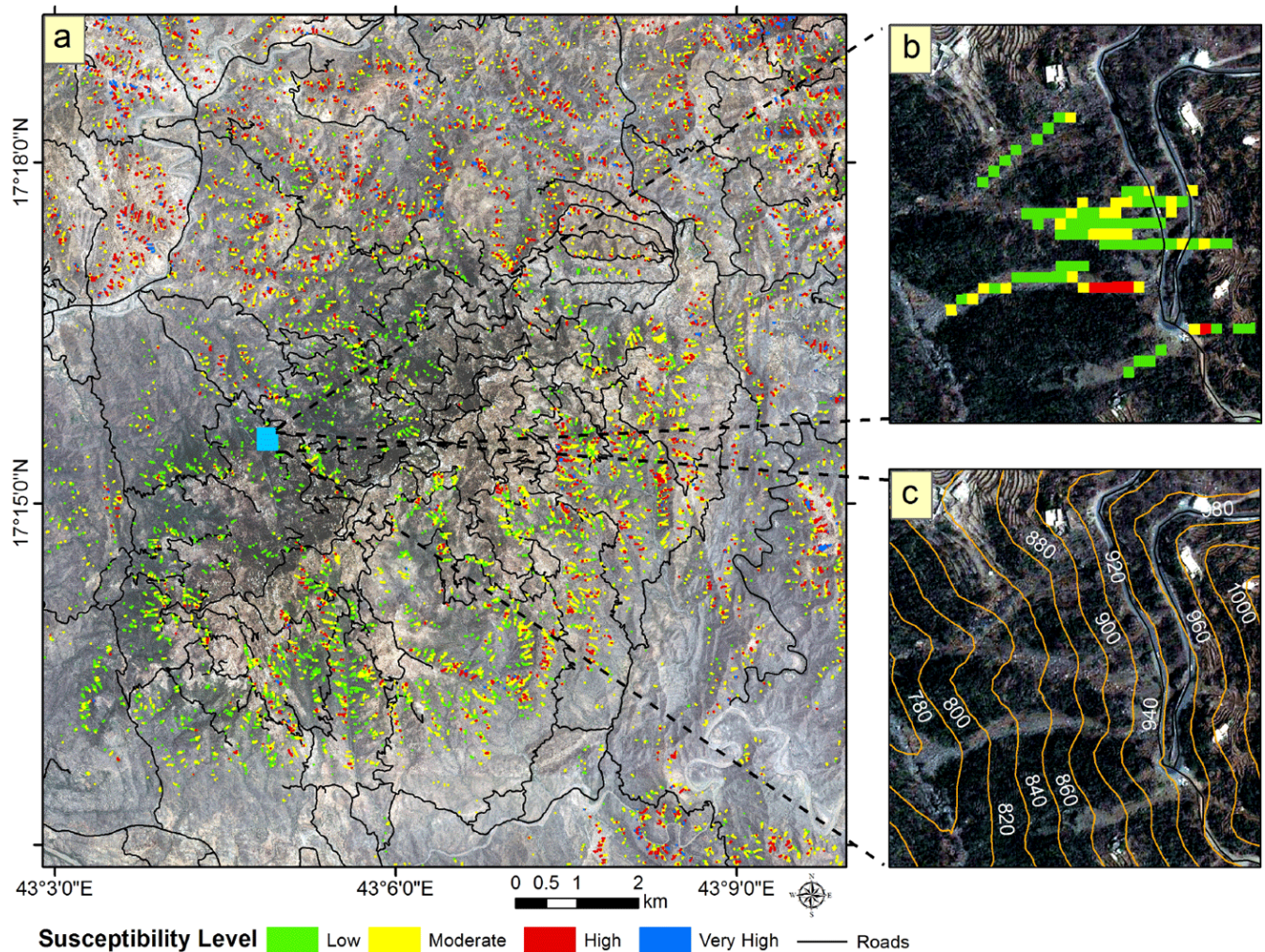


Figure 6. (a) Susceptibility map showing the susceptibility level for areas modeled as being prone to debris flow. (b) Enlargement of the boxed area in (a). (c) Same as (b), but with the modeled debris flow omitted. Note the correspondence between the modeled (b) and observed (c: bright areas) debris flows.

we can test for the first condition using remote sensing data, but not the second. Figure 7 shows 669 intersections with roads and 76 with houses; in these locations, slope failure could cause losses of human life and property. A field shot of one of these debris flows that intersects a road is shown in Fig. 4c. In the absence of high-spatial-resolution DEM data, a number of these identified intersections turned out to be false alarms. For example, we found in field trip 2 that a number of the identified house locations at intersections with debris streams were on higher ground than the streams that presumably intersect them. These types of false alarms were more pronounced for houses on high-ground elevations. Unfortunately, these observations cannot easily be extracted from available remote sensing data. Our field inspections during field trip 2 showed that all spaceborne debris flow/road intersections are valid, and approximately 60 % of the debris/house intersections are true.

Our field observations during field trips 1 and 2 for landslides (landslides 1–7, 11, 13, 14, 16, 18; Fig. 2a) and inspection of the distribution of these debris flows on Google Earth images showed that they are spatially correlated with the distribution of roads, and specifically asphalt roads, suggesting a causal effect. Many of them seem to originate from, or are enhanced by, the construction of roads. The debris flows are readily identified in Google Earth images. The flows have distinctly more rocks (bright tones) and less vegetation (dark tones), and thus they appear as bright areas compared to their surroundings (Fig. 6c). The following features support the suggestion that the debris flows are apparently enhanced by the construction of roads: (1) the majority of these flows originate downslope from roads; (2) debris flows often start as overland flows downslope from roads but quickly become organized in one or more streams away from the road; and

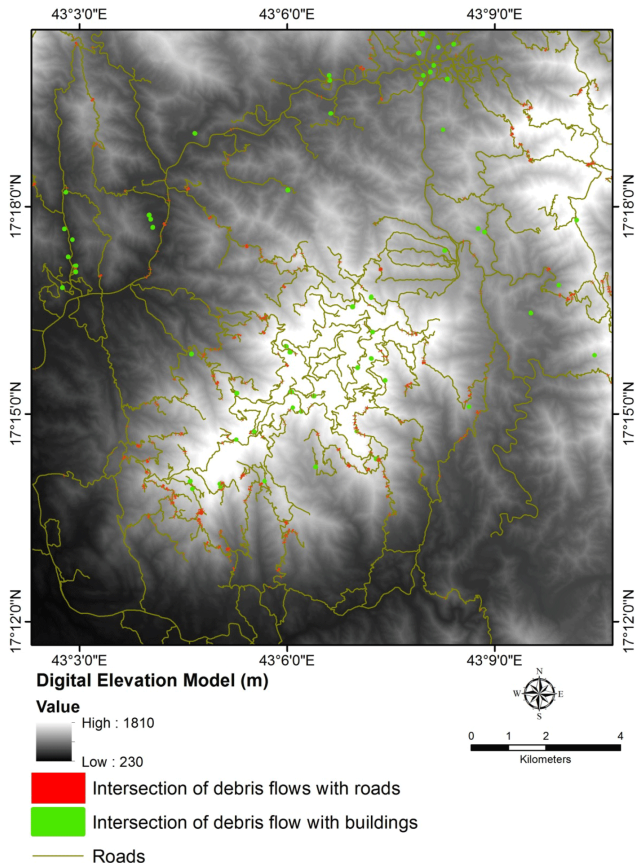


Figure 7. Map showing intersections of debris flows with roads and buildings.

(3) debris flows are more pronounced at higher elevations, at bends in roads, and along asphalt roads.

These observations and others across the entire Faifa area allowed us to develop a conceptual model for debris flow development. In this model, precipitation over the mountains is channeled toward asphalt roads by streams that intersect the roads or by overland flow over the mountainsides. Upon reaching the roads, the flows (either in streams or over the mountainsides) are often redirected to follow the gradient of the road instead of the gradient of the landscape. Once the road changes its orientation (e.g., at a bend), the flow on the road surface is redirected; at this time, the flow reverts to following the gradient of the landscape. The process is repeated as the flows intersect other roads downstream on their journey to the lowlands. Because asphalt roads – and to a lesser extent, unpaved roads (highly compacted material) – are impervious layers, they have the effect of impeding infiltration and enhancing runoff.

Landslides, when they do occur, modify the landscape. In a simple model, mass movement associated with a landslide will move mass downhill, deposit the transported mass downhill, and disrupt the general slope in the area. On a contour map, these features could give rise to (1) gentle slopes

as indicated by widely spaced, wiggly contours representing the chaotic surfaces formed by accumulated debris piling up downslope; and (2) steeper slopes represented by horseshoe-shaped, closely spaced contours uphill (Casals, 1986; Keaton and DeGraff, 1996). In Fig. 8, we outline a number of locations of possible historical landslides that display the relationships described above. In many of these locations, terraces were established. One interesting hypothesis worth investigating is that the locals targeted the areas of “mass deposition” within the ancient landslides to construct their terraces.

2.2.2 Landslides caused by failure along fracture planes

Many landslides result from failure along preexisting fracture planes (Lowell, 1990). Dip amount and dip direction are angular parameters that define the orientation of a discontinuity. The inclination of a plane below the horizontal is its dip angle (range: 0 to 90°), and its azimuth is its dip direction (range: 0 to 360°). The slope amount and slope direction are in reference to dip of the mountain face and the horizontal direction in which a mountain slope faces. When the slope amount is steeper than the dip of the discontinuity, the discontinuity surfaces are exposed on the face and sliding may occur (Norrish and Wyllie, 1996; Wyllie and Norrish, 1996). According to Norrish and Wyllie (1996), there are four necessary structural conditions for planar failure to occur. First, the strike of the planer discontinuity must be within 20° of the strike of the slope face. Second, the dip of the planer discontinuity must be less than the dip of the slope face and oriented in the same general direction. This condition does not apply to roads in the mountainous areas, where the road cut is usually a vertical wall. Third, the dip of the planer discontinuity must be greater than the angle of the friction of the surface. The ideal friction angle of the rock material is partially controlled by the size and shape of the grains exposed on the fracture surface and by the mass of the block above the planer discontinuity. Fine-grained rocks and rocks with high mica content tend to have a low friction angle, whereas coarse-grained rocks have a high friction angle (Norrish and Wyllie, 1996). For example, granite has a high friction angle that ranges from 34 to 40° (Barton, 1973, 1974; Jaeger and Cook, 1976; Wylie, 1992; Wyllie and Norrish, 1996). Finally, the lateral extent of the potential failure mass must be defined either by lateral release surfaces that do not contribute to the stability of the mass or by the presence of a convex slope shape that is intersected by the planar discontinuity (Norrish and Wyllie, 1996).

In this section, we use data collected along the major roads, our knowledge about the geology of the area, observations extracted from remotely acquired data, and GIS technologies to determine locations that are prone to movement along fracture planes.

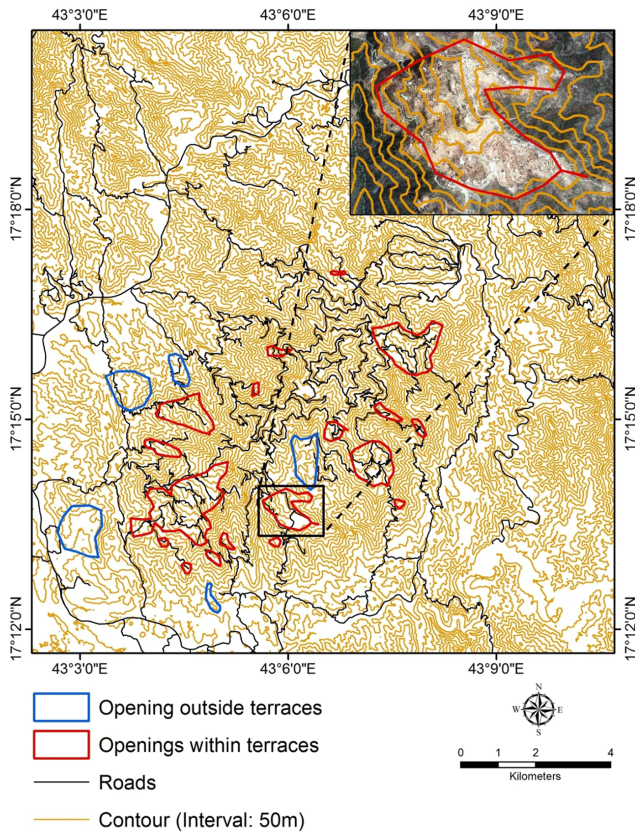


Figure 8. Contoured elevation map showing locations of possible historical landslides; these areas appear as domains of gentle slope surrounded by areas with steep slopes.

An intensive exercise was conducted along the major roads in Faifa to identify areas prone to mass movement along fracture planes. Ideally, one could extrapolate these measurements across the entire field area. Unfortunately, the measurements are limited in their areal distribution, making the application of simple extrapolation techniques an unreliable exercise. We made two main observations from the field (fracture plane dip direction and dip angle) and satellite-based measurements (ASTER, DEM, SIR-C) that led us to believe that our limited field measurements could be used to infer the dip angle and the direction of the fracture planes across large sections of the entire study area.

The first observation is that many of the slopes in the study area are apparently controlled by dominant fracture planes. This hypothesis was based on field observations made during our two field trips and on comparison of the slope direction of a particular pixel with the measured dip direction of the fracture planes measured in the examined pixel. Slopes controlled by fracture planes will dip in approximately the same direction. Thus, by identifying a particular slope direction that is consistently controlled by fracture planes dipping in the same direction, one can infer the presence of such fracture planes whenever that particular slope direction is

encountered in the field area. For each slope direction angle (1 to 360°), we reported the number of locations where measurements were made, the dip direction, and the dip angle for all fracture planes with a dip direction similar ($\pm 20^\circ$) to that of the slope in the examined pixel. As described earlier, the fracture plane dip angle and direction measurements were collected along transects covering the main roads in Faifa. For each transect, the major fracture plane directions were first identified; these ranged from one to five major fracture plane directions. For each of the identified major fracture plane directions, representative measurements were acquired, averaged, and reported.

For each transect, we compared the directions of the representative fracture planes with the slope direction. Two hundred and forty-three slope directions were identified along the examined transects, only 106 of which were found to have 1 or more fracture planes dipping in a similar ($\pm 20^\circ$) direction. A 50% success indicates that in half of the examined locations, we found fracture planes with dip directions similar to those of the investigated slope. The identified slopes were considered for extrapolation purposes only if consecutive (three or more) slope directions satisfied the above-mentioned condition. We set this condition because a prominent slope direction is rarely represented by a single and unique value and is more likely to be represented by a range of consecutive slope direction numbers. This statement applies to slope angle, fracture plane dip direction, and fracture plane dip angle. One or more factors could contribute to this, including (1) random variations in dip and slope directions and amounts, (2) human errors in collecting field measurements, and (3) averaging of measurements across the width and length of investigated pixels. The identified consecutive slopes were lumped in groups, where a group is represented by a range of slopes; these typically consisted of three to five consecutive numbers but could reach up to slope numbers in some cases (see Table 1, supplementary material). The slope 23 groups were then subdivided into subgroups on the basis of the dip angles of fracture planes. Typically, a group is subdivided into one to three subgroups. Average dip angles and directions were then obtained for each subgroup. Finally, we assigned fracture set information (average fracture plane directions and dip angles) to pixels with similar slope directions.

The second observation is that the overwhelming majority of the valleys in the study area were found to be structurally controlled. This finding was based on examination of ASTER VNIR, SIR-C, and DEM images that indicated that the majority of the valleys followed linear features, the orientation of which were found to be in four main directions: north–south, east–west, northwest–southeast, and northeast–southwest. We mapped the distribution of these zones using satellite imagery, DEM, and stream networks (Fig. 9). We also mapped 572 major weakness zones in the study area. Many of the field measurements for fracture planes within the fractured/faulted zones indicated that the strike of the

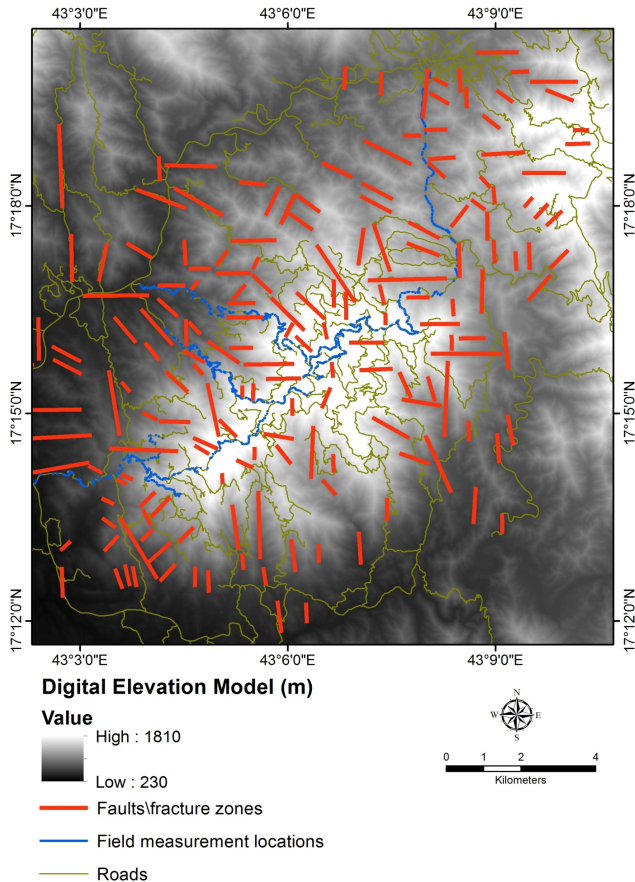


Figure 9. Distribution of the major zones of weakness (faults, fractures), sub-parallel and proximal fracture planes, and locations where field measurements (fracture plane orientations) were collected.

fracture planes was that of the fault or fracture zone. This observation allowed us to predict the presence of fracture planes within, and along the length of, the fractured/faulted zones that have the dip angle(s) and direction(s) of the fracture plane(s) measured within this zone. Our field- and satellite-based observations indicated that the longer the fracture zone, the greater its width; the zones varied in length from 93 to 2300 m and in width from 20 to 150 m.

Using the observations and methodologies described above, we were able to use the limited field observations in hand pertaining to the fracture plane orientation to infer the fracture plane orientations across large sectors of the Faifa area and surroundings. We generated a map that displays fracture plane dip angle(s) and direction(s) across the entire Faifa area. The accuracy of our predictions was assessed by repeating the extrapolation steps described above using a subset (433 records) of the available datapoints (559 records). The accuracy of the extrapolation technique was then assessed by comparing the predicted dip directions and amounts to those of the excluded 126 records. A prediction was considered to be successful if the predicted dip angle

and direction was similar (within 20°) to that of a proximal (< 10 m) record. Predicted values for 75 of the 126 field measurement were found to be successful (success rate: $\sim 60\%$).

The next step involved the use of the generated fracture plane map to extract a susceptibility map that shows the pixels that are prone to mass movement along the identified fracture planes (Fig. 10). To generate this susceptibility map we utilized (1) fracture amount and direction maps, (2) slope angle and direction maps, and (3) road distribution and orientation maps. A pixel is considered to be susceptible to failure along a planar discontinuity if the following conditions are met: (1) the strike of the planar discontinuity must be within 20° of the strike of the slope face; (2) the dip of the planar discontinuity must be less than the dip of the slope face; and (3) the dip of the planar discontinuity must be greater than the angle of the friction of the surface (40°). The selected angle of friction is based on laboratory testing of the shear strength of planar surfaces (mean: 39.6° for 29 measurements) within the study area. The measured mean value (39.6°) is consistent with reported shear strength values for granites (80% of outcrops in study area) collected from shear zones elsewhere (Barton, 1973; Jaeger and Cook, 1976). The last condition is waived along roads, because the road cuts in this steep mountainous area are near vertical. This distinction is reflected in Fig. 10, which displays two groups of areas that are susceptible to failure along planar discontinuities, areas located along roads (blue and yellow symbols), and others distant from the roads (red and green symbols).

3 Conclusions

We adopted an integrated (field and remote sensing) approach to accomplish the following in our test site, the Faifa mountain and surroundings in the Jazan area, Red Sea hills, Saudi Arabia: (1) identify the types and landslides and map their distribution, (2) identify the factors controlling landslide distribution, and (3) generate susceptibility maps outlining areas that are prone to the development of landslides. To compensate for the paucity of field data and the inaccessibility of the examined area, we adopted an approach that relies heavily on observations extracted from readily available remote sensing data sets and on the applications of GIS-based technologies to enable (1) spatial analyses of all relevant data sets (published data sets, derived products, and field data); and (2) extrapolation of the limited field observations that were acquired along the main roads across the entire field area. Debris flows within ephemeral valleys occur on steep slopes along channel networks in areas that are less vegetated than their surroundings; on contoured elevation maps (contour interval: 10 m), such areas show evidence of disruption of contours. The products (slope, channel network, and contoured elevations maps) that were used to extract the debris flow distribution in the study area were all derived from DEMs (contour interval: 10 m). Investigating

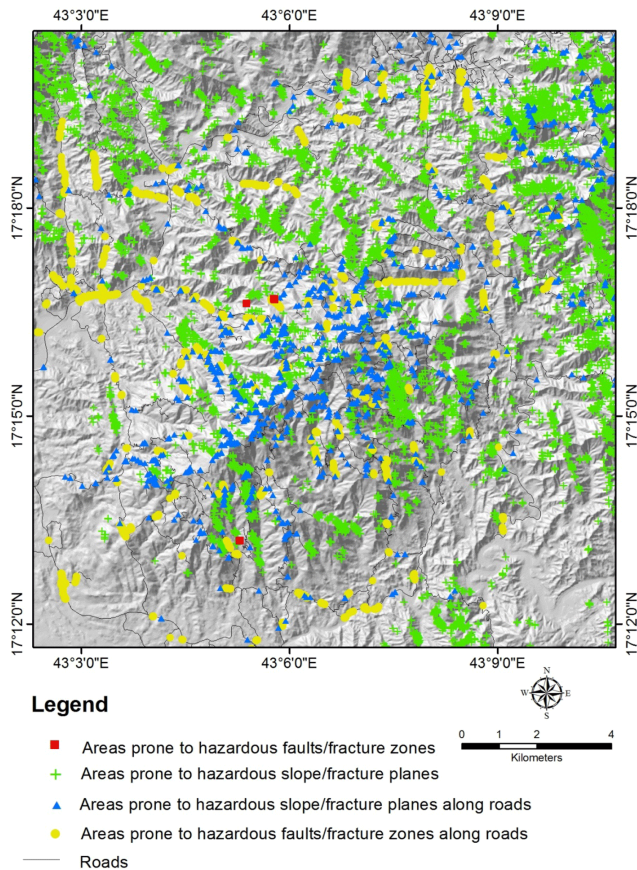


Figure 10. Susceptibility map showing the distribution of picture elements along (blue and yellow symbols), and away from (red and green symbols) roads that are susceptible to failure by motion along fracture planes. Information pertaining to the extrapolation technique that was applied to assign fracture set information to pixels is also provided in the figure; green and blue symbols refer to extrapolation related to “first observation”, and the red and yellow symbols are related to “second observation” (refer to Sect. 2.2.3).

the intensity of vegetation in an area was made possible by examining NDVI images that were extracted from SPOT multispectral images. Coverages depicting the distribution of roads and houses were used to evaluate whether the extracted debris flow distribution poses risks to the human population and properties.

Two main types of landslides were identified: the first is caused by debris flows within ephemeral valleys (Type I), and the second by failure along fracture planes (Type II). For the first type (Type I), steps 1 through 3 (listed above) were implemented by extracting NDVI and slope values over known locations of debris flows and using this data to define linear relationships that allow the identification of areas prone to developing debris flows elsewhere in the study area. In constructing debris flow susceptibility maps, additional constraints were specified: (1) minimum slopes of 30° for flows within ephemeral valleys; and (2) absence of terraces, structures that enhance infiltration and reduce runoff, making it less likely for debris flow to occur.

Comparisons between the distribution of predicted and observed debris flows show a success rate of 82 % in the case of the ephemeral valleys; the unverified debris flows are interpreted here as potential locations where debris flows could be triggered in the future. The debris flows pose a risk to human life and property; approximately 670 intersections with roads and 75 intersections with houses were mapped. All space-borne debris flow/road intersections were found to be valid, but only 60 % of the debris/house intersections were validated in the field.

For the second type of landslide (Type II), we took advantage of two main observations that allowed us to infer the dip angle and direction of the fracture planes across large sections of the entire study using a limited set of field measurements. These observations showed that (1) many of the slopes in the study area are apparently controlled by dominant fracture planes, and (2) many of the field measurements for fracture planes within the fractured/faulted zones indicated that the strike of the fracture plane was similar to that of the fault or fracture zone. The measured and inferred fracture plane orientations were then used to generate a susceptibility map showing pixels that are prone to mass movement along fracture planes. The fracture planes for these pixels have strike values that are within 20° of the strike of the slope face and have dip angles that exceed the angle of the friction but are less than the slope angles. The last condition is waived along roads, given that the road cuts are nearly vertical. We found 18 181 picture elements that satisfy these conditions. Because comparisons between the distribution of predicted and observed fracture plane orientations showed a success rate of 60 %, we suggest that the reliability of the generated susceptibility map is 60 % at best. The adopted methodology is best suited for the detection of areas prone to planar sliding, but not for topples and wedge sliding. For example, one of the adopted criteria for the detection of areas prone to failure along a fracture plane is the requirement that the dip direction is similar ($\pm 20^\circ$) to that of the slope. This is not necessarily required for topples and wedge sliding.

As is the case in the Faifa area, many landslide occurrences worldwide are reported from remote areas that are distant from urban centers and lack adequate infrastructure and road networks, areas of high relief and steep slopes, which makes such areas largely inaccessible. Under these conditions, monitoring landslide activities using traditional methodologies becomes a difficult and expensive exercise. The methodologies adopted in this study rely heavily on readily available global remote sensing data sets and utilize straightforward GIS technologies for spatial analysis of these data sets; therefore, they can offer reliable and cost-effective alternatives. A word of caution: the adopted approach should not be considered a substitute for traditional field-intensive methodologies and measurements, but should be only considered for inaccessible areas where obtaining detailed field measurements is difficult and/or cost prohibitive.

The Supplement related to this article is available online at doi:10.5194/nhess-14-1553-2014-supplement.

Acknowledgements. Funding for this project was provided through an award from the Saudi Geological Survey (SGS) to Western Michigan University (award SGS5/2141). The SGS also provided logistical support for conducting field work in the Jazan area.

Edited by: R. Lasaponara

Reviewed by: A. Lanorte and three anonymous referees

References

- Abou Ouf, M. A. and El Shater, A.: Sedimentology and mineralogy of Jizan shelf sediments, Red Sea, Saudi Arabia, *J. King Abdulaziz University*, 3, 133–141, 1992.
- Agar, R. A.: The Najd fault system revisited a two-way strike-slipogen in the Saudi Arabian Shield, *J. Struct. Geol.*, 9, 41–48, 1987.
- Alehaideb, I.: Rainfall distribution in the southwest of Saudi Arabia, Ph.D. thesis, Arizona State Univ., Arizona, USA, 430 pp., 1985.
- Barton, N. R.: Review of a new shear strength criterion for rock joints, *Eng. Geol.*, 7, 287–332, 1973.
- Barton, N. R.: A review of the shear strength of filled discontinuities in rock, *Norges Geotekniske Institutt*, 105, 1–19, 1974.
- Casals, J. F.: Analysis of a landslide along Interstate 70 near Vail, Master's thesis, Colorado School of Mines, Golden, Colo., USA, 121 pp., 1986.
- Chang, K.: Introduction to geographic information system, 3rd edition, McGraw Hill, New York, 432 pp., 2006.
- Cruden, D. and Varnes, D.: Landslide types and processes, in: *Landslides: Investigation and Mitigation*, Transportation Research Board, Washington, D.C., 36–75, 1996.
- Fairer, G. M.: Explanatory notes to the geologic map of the Wadi Baysh Quadrangle, Deputy Ministry for Mineral Resources, Ministry of Petroleum and Mineral Resources, Kingdom of Saudi Arabia, Denver, Colorado, USA, 1–23, 1985.
- Florsheim, J. L., Keller, E. A., and Best, D. W.: Fluvial sediment transport in response to moderate storm flows following chaparral wildfire, *Geol. Soc. Am. Bull.*, 103, 504–511, 1991.
- Garbrecht, J. and Martz, L. W.: TOPAZ Version 1.20: an automated digital landscape analysis tool for topographic evaluation, drainage identification, watershed segmentation and sub-catchment parameterization, *Grazinglands Research Laboratory*, El Reno, Oklahoma, 1–21, 1997.
- Horton, R. E.: The role of infiltration in the hydrologic cycle, *EOS T. Am. Geophys. Un.*, 14, 446–460, 1933.
- Hutchinson, J.: Morphological and geotechnical parameters of landslides in relation to geology and hydrogeology, *Fifth International Symposium on Landslides*, 10–15 July 1988, Rotterdam, the Netherlands, 3–35, 1988.
- Jackson, R. D. and Huete, A. R.: Interpreting vegetation indices, *Prev. Vet. Med.*, 2, 185–200, 1991.
- Jaeger, J. C. and Cook, N. G. W.: *Fundamentals of Rock Mechanics*, 2nd edition, Chapman and Hall, London, UK, 593 p., 1976.
- Keaton, J. R. and DeGraff, J. V.: Surface observation and geologic mapping, in: *Landslides: Investigation and Mitigation*, Transportation Research Board, Washington, D.C., 178–230, 1996.
- Lowell, S.: The K M Mountain landslide near Skamokawa, *Washington Geologic Newsletter*, 18, 3–7, 1990.
- Naderman, G. C., Hansard, J. R., and Denton, H. P.: Surface water management for crop production on highly erodible land, *Appl. Agr. Res.*, 5, 243–254, 1990.
- Norrish, N. I. and Wyllie, D. C.: Rock slope stability analysis, in: *Landslides: Investigation and Mitigation*, Transportation Research Board, Washington, D.C., 391–425, 1996.
- Rouse, J.: Monitoring the Vernal Advancement and Retrogradation (Green Wave Effect) of Natural Vegetation, *Remote Sens.*, 36, 4–38, 1973.
- Scott, K.: *Origin and Sedimentology of 1969 Debris Flows Near Glendora, California*, *Geol. Surv. Prof. Paper 750*, United States Government Printing Office, Washington, 242–247, 1971.
- Stoeser, D. B. and Camp, V. E.: Pan-African microplate accretion of the Arabian Shield, *Geol. Soc. Am. Bull.*, 96, 817–827, 1985.
- Weirich, F.: The generation of turbidity currents by subaerial debris flows, *California, Geol. Soc. Am. Bull.*, 101, 278–291, 1989.
- Wells, W., Wohlgenuth, P., Campbell, A., and Weirich, F.: Post-fire Sediment Movement by Debris Flows in the Santa Ynez Mountains, California, *Corvallis Symposium, International Association of Hydrologic Sciences Corvallis*, 3–7 August 1987, Corvallis, Oregon, 275–276, 1987.
- Wolfenden, E., Ebinger, C., Yirgu, G., Deino, A., and Ayele, D.: Evolution of the Northern Main Ethiopian Rift: birth of a triple junction, *Earth Planet. Sc. Lett.*, 224, 213–228, 2004.
- Wyllie, D. C.: *Foundations on Rock*, 1st edition, Chapman and Hall, London, UK, 331 pp., 1992.
- Wyllie, D. C. and Norrish, N. I.: Rock strength properties and their measurement, in: *Landslides: Investigation and Mitigation*, Transportation Research Board, Washington, D.C., 372–379, 1996.